

Experimental Measurements of Ion Heating in Collisional Plasma Shocks and Interpenetrating Supersonic Plasma Flows

Samuel J. Langendorf,^{1,*} Kevin C. Yates,^{2,1} Scott C. Hsu,^{1,†} Carsten Thoma,³ and Mark Gilmore²

¹*Los Alamos National Laboratory, Los Alamos, NM 87545*

²*University of New Mexico, Albuquerque, NM 87131*

³*Voss Scientific, Albuquerque, NM 87108*

(Dated: March 4, 2019)

We present direct measurements of ion heating due to collisional plasma shocks and interpenetrating supersonic plasma flows, which are formed by the oblique merging of two coaxial-gun-formed plasma jets. Our study was repeated using four jet species: N, Ar, Kr, and Xe. In conditions with small interpenetration between jets, the observed peak ion temperature T_i is consistent with the predictions of collisional plasma-shock theory, showing a substantial elevation of T_i above the electron temperature T_e and also the subsequent decrease of T_i on the classical ion–electron temperature-equilibration time scale. In conditions of significant interpenetration between jets, such that shocks do not apparently form, the observed peak T_i is still appreciable and greater than T_e , but much lower than that predicted by collisional plasma-shock theory. Experimental results are compared with multi-fluid plasma simulations.

Shocks are a fundamental feature of supersonic plasma flows and affect the detailed energy balance and dynamical evolution of physical systems in which the shocks are embedded, e.g., in astrophysical systems [1–4] or in the laboratory, as in high-energy-density (HED) [5] or inertial-confinement-fusion (ICF) [6] experiments. Differing fundamentally in two key respects from hydrodynamic shocks, plasma shocks (1) can be mediated either by classical Coulomb collisions between plasma particles (collisional plasma shock [7, 8]) or by collective effects such as the Weibel instability [9–11] (collisionless plasma shock [12]), and (2) are more complex due to the presence and coupled interactions of electrons, ions (sometimes multiple species), electromagnetic fields, and radiative and equation-of-state (EOS) effects. This Letter focuses on unmagnetized collisional plasma shocks and interpenetrating supersonic plasma flows, in which radiative and thermal losses and EOS effects cannot be ignored *a priori*. Related recent experiments include colliding plasmas formed by plasma railguns [13–15], wire-array Z pinches [16, 17], and laser ablation of solid targets [18]. The latter are also being used to study collisionless shocks [19–22]. The study of interpenetrating, colliding plasma flows has a long history, e.g., [23–25].

This Letter presents the first detailed and comparative experimental diagnostic study of ion heating due to unmagnetized collisional plasma shocks and interpenetrating supersonic plasma flows. Our experiments are repeated using N, Ar, Kr, and Xe, and the observed ion heating is a sensitive measure of the underlying coupled physics. Some prior experiments studying plasma shocks and interpenetrating flows have reported isolated measurements of ion temperature T_i inferred from multi-parameter fits to Thomson-scattering spectra, e.g., ablation phase of a wire-array Z pinch [26], collisionless counter-streaming of laser-produced CH plasmas [21, 27], and development of a collisional strong shock formed via

expanding Si and N plasma into H₂ gas [18]. Our T_i measurements are inferred directly from Doppler broadening of ion line emission. Detailed measurements of the time evolution of T_i within the post-shock or jet-interpenetration regions imply impulsive heating followed by slower equilibration with the electron temperature T_e . The latter remains much lower than T_i , as inferred from comparisons between broadband visible line spectra and atomic modeling. The results presented here constitute new fundamental data for unmagnetized collisional plasma shocks and interpenetrating supersonic plasma flows, and may be uniquely valuable for validating first-principles modeling, e.g., [28–30], of these phenomena, which are crucial for accurate modeling of HED and ICF experiments. At present, there are significant disagreements among different codes and models [31, 32]. Our experiments were motivated by and are of importance for evaluating the effects of collisional plasma shocks on plasma-liner formation via merging plasma jets as a potential magneto-inertial-fusion driver [33, 34].

The results presented here were obtained on the Plasma Liner Experiment (PLX) [34, 35], where six recently developed coaxial plasma guns [34, 36] are mounted on a 2.74-m-diameter spherical vacuum chamber. In these experiments, two plasma jets are fired at a time to provide an unobstructed view of the jet-merging dynamics, with merging half-angle $\theta = 11.6^\circ$ or 20.5° , as shown in Figs. 1(a) and 1(b), respectively. At the exit of the gun nozzle, each jet has ion density $n_i \sim 2 \times 10^{16} \text{ cm}^{-3}$, $T_e \approx T_i \approx 1.5 \text{ eV}$, mean-charge $\bar{Z} \approx 1$, diameter $\approx 8.5 \text{ cm}$, and speed $v_{\text{jet}} \approx 25\text{--}80 \text{ km/s}$ [34]. Details of the plasma-gun design and jet characterization are reported elsewhere [34, 36]. Extensive prior work [13, 14, 37] showed that, as a jet propagates over $\sim 1 \text{ m}$, it expands radially and axially at approximately the internal sound speed C_s , T_e and v_{jet} stay approximately constant, n_i decreases consistent with mass con-

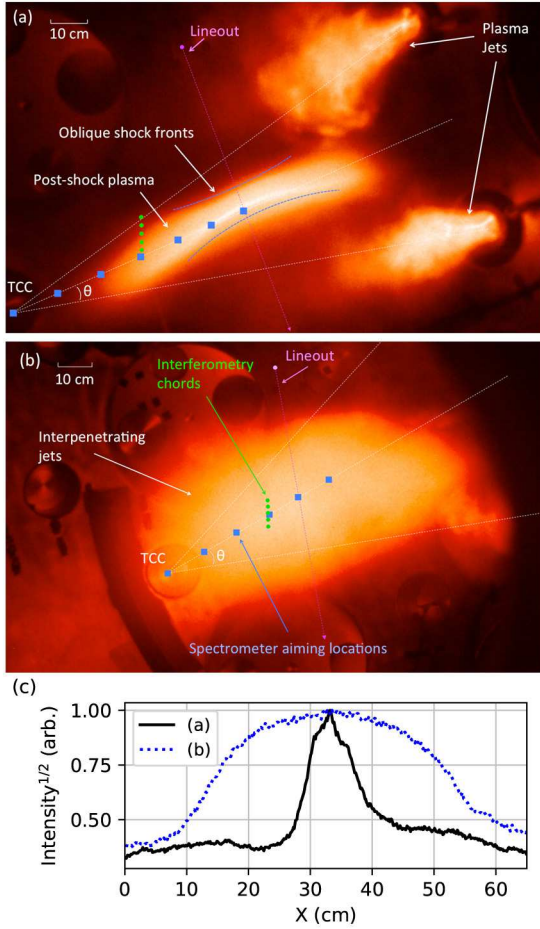


FIG. 1. Fast-camera, visible-light images (10-ns exposure, log intensity, false color) of two merging N plasma jets with (a) $\theta = 11.6^\circ$ (shot 2559, $t = 38 \mu\text{s}$), showing the formation of oblique, collisional plasma shocks and post-shock plasma (labeled notionally), and (b) $\theta = 20.5^\circ$ (shot 1570, $t = 36 \mu\text{s}$), showing Ar jet-jet interpenetration (large region of diffuse emission) without apparent shock formation. Diagnostic chord positions (green dots and blue squares) and target-chamber center (TCC) are shown. (c) Lineouts of the square root of intensity correspond to the blue, dotted lines in (a) and (b).

servation, the magnetic field strength decays by $1/e$ every few μs such that both the thermal pressure and kinetic energy density (of the jet directed motion) dominate over the magnetic pressure by the time the jets merge, and that density jumps and jet-merging morphology are consistent with oblique collisional shock formation.

The plasma parameters reported in this work, i.e., T_i , T_e , electron density n_e , \bar{Z} , and v_{jet} , are inferred from diagnostic measurements (positions shown in Fig. 1). Plasma T_i is measured via Doppler broadening of plasma ion line emission using a high-resolution, 4-m McPherson monochromator (2062DP) with a 2400 mm^{-1} grating and a single-frame intensified charge-coupled-device (CCD) detector. The spectral resolution is 1.5 pm/pixel

at the typical visible wavelengths of interest, sufficient to resolve $T_i \gtrsim$ a few eV for Xe and correspondingly smaller values for lighter species. The high-resolution spectrometer records two chords at a time with typical waist diameter of 2 cm; chord positions are indicated by the blue squares (10-cm separation) in Fig. 1. Doppler broadening is the primary source of line broadening in our parameter regime, and the effects of differing Doppler shifts of different jets are minimized by viewing the merging at $\approx 90^\circ$ relative to the directions of jet propagation. Turbulent motion of the merged plasma is not indicated in the experimental images. Line-integrated measurements of n_e are obtained using a multi-chord laser interferometer [38]. The density of the post-shock or jet-interpenetration regions are measured using five interferometry chords (0.3-cm chord diameter and 1.5-cm spacing between chords) 30 cm from target-chamber center (TCC), as shown by the green dots in Fig. 1. Plasma T_e and \bar{Z} are bounded [37] by comparing broadband visible spectroscopy data [34], obtained along the same chord positions as the interferometry (green dots in Fig. 1 but with 1-cm chord diameter), to atomic modeling and using the inferred n_e from interferometry. Jet speeds are measured via a photodiode array at the end of each gun nozzle [34]. A fast-framing camera with an intensified CCD (PCO dicam pro) obtains visible-light images of the shock formation or jet interpenetration. Further details of the PLX facility, coaxial plasma guns, diagnostics, and plasma-jet parameters are described in Ref. 34.

Figures 1(a) and 1(b) show fast-camera images of two jets merging with $\theta = 11.6^\circ$ and 20.5° , respectively, and Fig. 1(c) shows lineouts of the square root of intensity across the region of jet merging. If T_e is nearly spatially uniform, which is consistent with both collisional plasma-shock theory [8] and our experimental measurements, then the lineouts in Fig. 1(c) are representative of the n_i profile. For the black curve, the gradient scale length \sim few cm, which is consistent with oblique collisional plasma-shock thicknesses (discussed later).

Figure 2(a) shows representative interferometry profiles of line-integrated n_e in the post-merged plasma. These measurements show small spatial variations in the post-merge region and are used to infer post-merge n_e . Figure 2(b) shows the broadband emission spectrum (from the same shot) compared to PrismSPECT modeling [39], which we use to bound T_e and \bar{Z} . In this case, the best fit is $T_e = 1.9 \text{ eV}$ and $\bar{Z} = 1.0$ for $n_e = 3 \times 10^{14} \text{ cm}^{-3}$. The bounds on T_e and \bar{Z} are determined based on the absence and/or presence of certain lines in the data as compared to the PrismSPECT modeling [37]. All post-merge values of n_e , T_e , and \bar{Z} are summarized in Table I. The broadband spectra also reveal that no impurity lines are observed during the first $10 \mu\text{s}$ of jet merging, and therefore we do not expect the results in Table I to be affected by impurities.

The primary result of this work is the measurement

TABLE I. Summary of experimental parameters. The n_e , T_e , \bar{Z} , and ion-ion mean free path λ_i are experimentally inferred post-merge values. The jet-jet interpenetration length $L_{ii,s}$ [see Eq. (1)], counter-streaming speed $v = 2v_{jet} \sin \theta$, and jet Mach number $M = v/[\gamma k(T_i + \bar{Z}T_e)/m_i]^{1/2}$ are calculated using estimated pre-merge plasma parameters.

Case	(a)	(b)	(c)	(d)	(e)	(f)	(g)	(h)
Half-angle θ	11.6°	11.6°	11.6°	11.6°	20.5°	20.5°	20.5°	20.5°
Species	Ar	Xe	N	Kr	Ar	Xe	N	Kr
v_{jet} (km/s)	41.5	24.3	44.8	64.8	42.1	27.4	52.2	57.0
v (km/s)	16.7	9.8	18.1	26.1	29.4	19.2	36.5	39.8
n_e (10^{14} cm^{-3})	4.0	4.8	4.6	3.8	4.6	13	8.9	11.6
T_e (eV)	2.0	1.7	1.7	1.4	2	1.7	2.6	1.4
\bar{Z}	1.0	1.2	1.0	1.0	1.0	1.2	1.1	1.0
$L_{ii,s}$ (cm)	2.8	3.0	0.2	49.8	30	21.2	4.9	168.1
λ_i (cm)	1.9	1.6	0.5	2	3.3	1.4	0.4	2.6
M	4.2	4.9	2.9	11.3	7.4	9.5	4.7	17.2

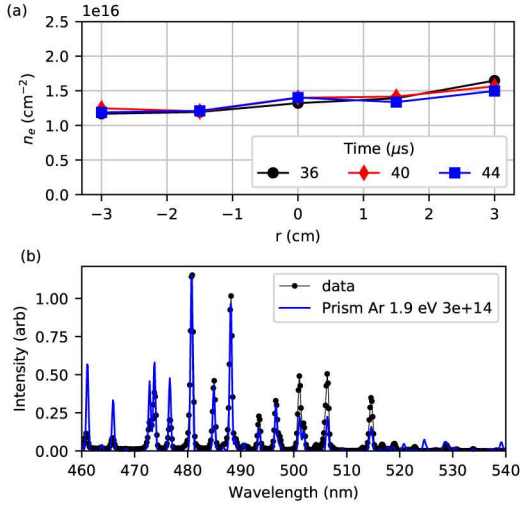


FIG. 2. (a) Line-integrated electron density, at the three indicated times, of interpenetrating Ar plasma jets (shot 1579, $\theta = 20.5^\circ$), as measured by interferometry [green dots in Fig. 1(b)], where $r < 0$ is below the midplane. (b) Visible spectral emission from merged plasma jets (shot 1579, $t = 38 \mu\text{s}$, 30 cm from TCC) and calculated spectra using PrismSPECT [39].

of the time evolution of T_i , as inferred from Doppler broadening of ionized emission lines, in the post-shock plasma or the region of jet-jet interpenetration as shown in Figs. 1(a) and 1(b), respectively. An example of the inference of T_i from Doppler spectroscopy data is shown in Fig. 3. Data at the earliest stage of jet merging show evidence of multiple overlapping line shapes (not shown here), which we believe to be due to interpenetration and systematic gun-angle-dependent Doppler shifts. These features are not observed several μs later into the jet merging. In data processing, we reject multiple-line-shape cases and include only the cases that satisfy a threshold goodness-of-fit to a single Gaussian.

Figures 4(a) and 4(b) show the inferred T_i versus time for the oblique merging of two jets with $\theta = 11.6^\circ$ and

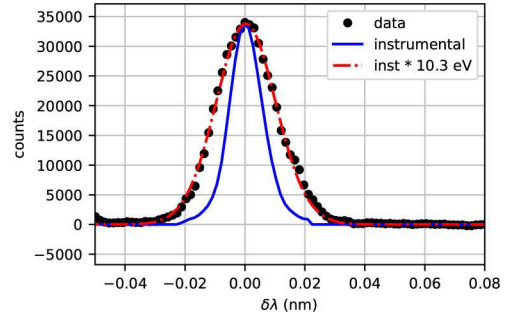


FIG. 3. Example of high-resolution spectroscopy data and fitting to infer $T_i = 10.3 \text{ eV}$ based on the best fit of the convolution of instrumental broadening with a Gaussian function (shot 1601, $t = 32 \mu\text{s}$, $1\text{-}\mu\text{s}$ gate, $\theta = 11.6^\circ$, Ar II 480.6-nm line, 30 cm from TCC, fitting error = $\pm 0.26 \text{ eV}$).

$\theta = 20.5^\circ$, respectively, and for the different species N, Ar, Kr, and Xe. The specific emission lines used were 463.0-nm N II, 480.6-nm Ar II, 473.9-nm Kr II, and 529.2-nm Xe II. In obtaining this high-resolution-spectroscopy dataset at the positions indicated by the blue squares in Figs. 1(a) and 1(b), we recorded progressively later times as we moved the spectrometer viewing chords closer to TCC (over multiple shots) because the jets and merged plasma move from right to left in Figs. 1(a) and 1(b). All recorded data meeting the goodness-of-fit criterion are included in Fig. 4.

To interpret the T_i measurements, first we consider the interpenetration distance $L_{ii,s}$ between jets upon merging. Depending on jet parameters and θ , $L_{ii,s}$ varies from much smaller to much larger than the characteristic jet spatial scale of a few tens of centimeters. Using estimated pre-merge jet parameters (v_{jet} from photodiodes, n_i decreased from measured post-merge $n_i = n_e/\bar{Z}$ by a factor of 2.5 for interpenetrating cases and 3.5 for shock-forming cases, and $T_i = T_e$ as inferred from spectroscopy) and a test-particle analysis [40], i.e., of a test ion from one jet penetrating the field particles of the opposing jet,

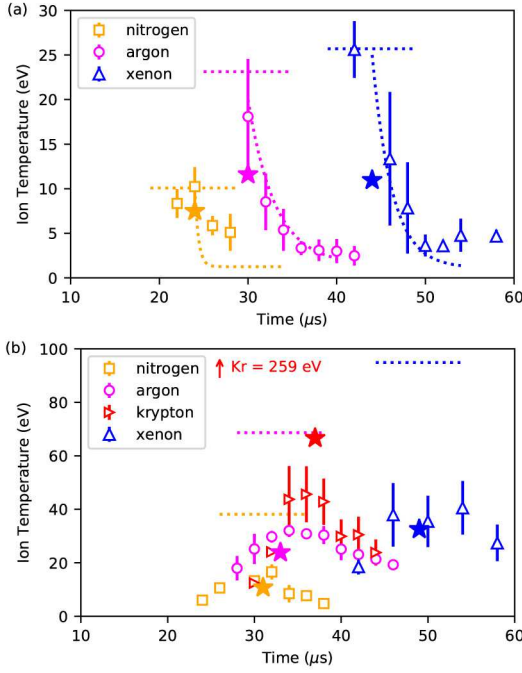


FIG. 4. Measured T_i , inferred from Doppler spectroscopy, vs. time for (a) $\theta = 11.6^\circ$ [shot ranges 1594–1625, 1744–1776, and 2606–2620, corresponding to cases (a)–(c) of Table I], for which collisional conditions are inferred, and (b) $\theta = 20.5^\circ$ [shot ranges 1563–1593, 1717–1743, 2139–2169, and 2271–2307, corresponding to cases (e)–(h) of Table I], for which significant interpenetration is inferred. Error bars indicate $\pm 1\sigma$ of shot-to-shot variations across ≈ 5 shots per data point. Horizontal dotted lines denote peak T_i based on Eq. (2); result for Kr in (b) is off scale as indicated. Stars indicate peak T_i from 1D-equivalent multi-fluid simulations (see text; placement of stars along the x-axis is not intended to reflect the simulation time). Dotted lines overlaying the data in (a) are the predictions of Eq. (3). The T_e remains $\lesssim 2$ eV in all cases (see Table I).

we estimate

$$L_{ii,s} = \frac{v}{4\nu_{ii,s}} = \frac{v}{4} \left[9 \times 10^{-8} n_{ii} \Lambda_{ii} \left(\frac{2}{\mu} \right) \frac{\mu^{1/2}}{\epsilon^{3/2}} \right]^{-1}, \quad (1)$$

where $v = 2v_{\text{jet}} \sin \theta$ (cm/s) is the counter-streaming speed between the two jets, $\nu_{ii,s}$ the counter-streaming ion–ion slowing frequency in the fast limit ($\gg \nu_{ie,s}$ for our parameters), Λ_{ii} the Coulomb logarithm for counter-streaming ions in the presence of warm electrons [14, 40], μ the ion/proton mass ratio, ϵ (eV) the energy associated with v , \bar{Z} (pre-merge) is assumed to be unity, and the factor of 4 in the denominator accounts for the integral effect of slowing down [41]. For $\theta = 11.6^\circ$ [Figs. 1(a) and 4(a)], $L_{ii,s} \sim 1$ cm, which is much smaller than the jet length ~ 30 cm. When $\theta = 20.5^\circ$ [Figs. 1(b) and 4(b)], $L_{ii,s} \sim v\epsilon^{3/2} \sim v^4$ increases accordingly to ~ 20 cm [columns (e)–(h) of Table I].

If $L_{ii,s}$ is small relative to the characteristic jet scale, collisional oblique plasma shocks form, as previously

shown [13, 14]. An upper bound for the jump in T_i across the shock, assuming that all of the heating goes to the ions, and T_e is uniform across the shock, is [42, 43]

$$\frac{T_{i2}}{T_{i1}} = \left[1 + \frac{2(\gamma - 1)}{(\gamma + 1)^2} \frac{\gamma M^2 + 1}{M^2} (M^2 - 1) \right] (\alpha + 1) - \alpha, \quad (2)$$

where subscripts ‘1’ and ‘2’ refer to pre- and post-shock, respectively, $\gamma = 5/3$ is the polytropic index, pre-shock Mach number $M \equiv v/[\gamma k(T_i + \bar{Z}T_e)/m_i]^{1/2}$, $\alpha \equiv (\bar{Z}T_e)/T_{i1}$, and $T_{i1} = T_e$ is assumed. Predicted T_{i2} based on Eq. (2) are plotted as horizontal dotted lines in Fig. 4. It is seen that the measured peak T_i agrees (within error bars) with the predicted T_i for Fig. 4(a) ($\theta = 11.6^\circ$), corresponding to the small-interpenetration cases of columns (a)–(c) of Table I. In these cases, the estimated post-shock ion–ion mean free paths are $\lambda_i \sim 0.1$ – 1 cm, consistent with the sharp jumps of the solid black curve of Fig. 1(c) representing collisional plasma shocks. On the other hand, in cases (d) (Kr at $\theta = 11.6^\circ$) and (e)–(f) ($\theta = 20.5^\circ$) of Table I, the conditions correspond to large interpenetration, and the T_i predicted by Eq. (2) is much higher than the measured peak T_i , as shown in Fig. 4(b). In these cases, it appears that oblique shocks do not form [see blue dotted curve of Fig. 1(c)]. In the particular case of Kr and $\theta = 11.6^\circ$ [case (d) of Table I], v_{jet} was higher than intended, and therefore interpenetration was the result.

The predicted, classical ion–electron temperature relaxation rate [40],

$$\frac{dT_i}{dt} = \left[1.8 \times 10^{-19} \frac{(m_i m_e)^{1/2} Z_i^2 n_e \Lambda_{ie}}{(m_i T_e + m_e T_i)^{3/2}} \right] (T_e - T_i), \quad (3)$$

is also plotted in Fig. 4(a) (overlaying the data). The prediction agrees well with the data, particularly for Ar and Xe, suggesting that the plasma shock predominantly heats the ions, followed by classical equilibration with the much colder electrons. For interpenetrating flows, heating and equilibration occur over similar time scales and does not admit a comparison based on Eq. (3).

Finally, we perform 1D, multi-fluid calculations (Lagrangian particles advect electron- and two ion-fluid quantities) of peak T_i (stars in Fig. 4) using the Chicago code [44, 45], including thermal/radiative losses and tabular EOS. For the collisional case [Fig. 4(a)], calculated peak T_i are lower than the collisional shock-jump prediction (expected with inclusion of thermal/radiative losses) but also somewhat lower than the data. For interpenetrating cases [Fig. 4(b)], the calculated peak T_i agree reasonably well with the data. Discrepancies with the data suggest further, detailed validation studies.

In conclusion, we have reported a comprehensive experimental study of ion heating in collisional plasma shocks and interpenetrating supersonic plasma flows formed by the oblique merging of two laboratory plasma

jets. The experiments were repeated for four jet species: N, Ar, Kr, and Xe. The post-merge $T_i \gg T_e$ in all cases investigated, including for both very small and substantial jet interpenetration, indicating that the predominant heating goes to the ions for both cases. For cases with shock formation, the measured peak T_i agrees well with the theoretically predicted T_i jump for a collisional plasma shock [Eq. (2)]. For cases with substantial interpenetration, the measured peak T_i , unsurprisingly, is substantially below that predicted by the collisional plasma-shock theory. The predicted classical ion–electron temperature relaxation compares well with the observed T_i decay in shock-forming cases. Multi-fluid Chicago simulations show some agreement with the peak- T_i data in both shock-forming and interpenetrating cases; the differences highlight an opportunity for detailed model validation for this and other codes being used to improve our understanding of HED and ICF experimental results.

We acknowledge J. Dunn, E. Cruz, A. Case, F. D. Witherspoon, S. Brockington, J. Cassibry, R. Samulyak, P. Stoltz, Y. C. F. Thio, and D. Welch for technical support and/or useful discussions. This work was supported by the Office of Fusion Energy Sciences and the Advanced Research Projects Agency–Energy of the U.S. Dept. of Energy under contract no. DE-AC52-06NA25396.

* samuel.langendorf@lanl.gov

† scotthsu@lanl.gov

- [1] R. Blandford and D. Eichler, *Phys. Rep.* **154**, 1 (1987).
- [2] A. Bell, *Mon. N. Roy. Astron. Soc.* **182**, 147 (1978).
- [3] D. Ryu, H. Kang, E. Hallman, and T. Jones, *Astrophys. J.* **593**, 599 (2003).
- [4] M. Markevitch, A. Gonzalez, L. David, A. Vikhlinin, S. Murray, W. Forman, C. Jones, and W. Tucker, *Astrophys. J. Lett.* **567**, L27 (2002).
- [5] R. P. Drake, *High-Energy-Density Physics* (Springer, Berlin, 2006).
- [6] S. Atzeni and J. Meyer-ter-Vehn, *The Physics of Inertial Fusion* (Oxford University Press, New York, 2004).
- [7] J. D. Jukes, *J. Fluid Mech.* **3**, 275 (1957).
- [8] M. Y. Jaffrin and R. F. Probstein, *Phys. Fluids* **7**, 1658 (1964).
- [9] E. S. Weibel, *Phys. Rev. Lett.* **2**, 83 (1959).
- [10] W. Fox, G. Fiksel, A. Bhattacharjee, P.-Y. Chang, K. Germaschewski, S.X. Hu, and P.M. Nilson, *Phys. Rev. Lett.* **111**, 225002 (2013).
- [11] C. M. Huntington, F. Fiuza, J. S. Ross, A. B. Zylstra, R. P. Drake, D. H. Froula, G. Gregori, N. L. Kugland, C. C. Kuranz, M. C. Levy, C. K. Li, J. Meinecke, T. Morita, R. Petrasso, C. Plechaty, B. A. Remington, D. D. Ryutov, Y. Sakawa, A. Spitkovsky, H. Takabe, and H.-S. Park, *Nature Phys.* **11**, 173 (2015).
- [12] D. A. Tidman and N. A. Krall, *Shock Waves in Collisionless Plasmas* (Wiley, New York, 1971).
- [13] E. C. Merritt, A. L. Moser, S. C. Hsu, J. Loverich, and M. Gilmore, *Phys. Rev. Lett.* **111**, 085003 (2013).
- [14] E. C. Merritt, A. L. Moser, S. C. Hsu, C. S. Adams, J. P. Dunn, A. Miguel Holgado, and M. A. Gilmore, *Phys. Plasmas* **21**, 055703 (2014).
- [15] A. L. Moser and S. C. Hsu, *Phys. Plasmas* **22**, 055707 (2015).
- [16] G. Swadling, S. Lebedev, N. Niasse, J. Chittenden, G. Hall, F. Suzuki-Vidal, G. Burdiak, A. Harvey-Thompson, S. Bland, P. De Grouchy, E. Khoory, L. Pickworth, J. Skidmore, and L. Suttle, *Phys. Plasmas* **20**, 022705 (2013).
- [17] G. F. Swadling, S. V. Lebedev, A. J. Harvey-Thompson, W. Rozmus, G. C. Burdiak, L. Suttle, S. Patankar, R. A. Smith, M. Bennett, G. N. Hall, F. Suzuki-Vidal, and J. Yuan, *Phys. Rev. Lett.* **113**, 035003 (2014).
- [18] H. G. Rinderknecht, H.-S. Park, J. S. Ross, P. A. Amendt, D. P. Higginson, S. C. Wilks, D. Haberberger, J. Katz, D. H. Froula, N. M. Hoffman, G. Kagan, B. D. Keenan, and E. L. Vold, *Phys. Rev. Lett.* **120**, 095001 (2018).
- [19] L. Romagnani, S. V. Bulanov, M. Borghesi, P. Audebert, J. C. Gauthier, K. Lowenbruck, A. J. Mackinnon, P. Patel, G. Pretzler, T. Toncian, and O. Willi, *Phys. Rev. Lett.* **101**, 025004 (2008).
- [20] Y. Kuramitsu, Y. Sakawa, T. Morita, C. D. Gregory, J. N. Waugh, S. Dono, H. Aoki, H. Tanji, M. Koenig, N. Woolsey, and H. Takabe, *Phys. Rev. Lett.* **106**, 175002 (2011).
- [21] J. Ross, S. Glenzer, P. Amendt, R. Berger, L. Divol, N. Kugland, O. Landen, C. Plechaty, B. Remington, D. Ryutov, W. Rozmus, D. H. Froula, G. Fiksel, C. Sorce, Y. Kuramitsu, T. Morita, Y. Sakawa, H. Takabe, R. P. Drake, M. Grosskopf, C. Kuranz, G. Gregori, J. Meinecke, C. D. Murphy, M. Koenig, A. Pelka, A. Ravasio, T. Vinci, E. Liang, R. Presure, A. Spitkovsky, F. Miniati, and H.-S. Park, *Phys. Plasmas* **19**, 056501 (2012).
- [22] J. S. Ross, D. P. Higginson, D. Ryutov, F. Fiuza, R. Hatarik, C. M. Huntington, D. H. Kalantar, A. Link, B. B. Pollock, B. A. Remington, H. G. Rinderknecht, G. F. Swadling, D. P. Turnbull, S. Weber, S. Wilks, D. H. Froula, M. J. Rosenberg, T. Morita, Y. Sakawa, H. Takabe, R. P. Drake, C. Kuranz, G. Gregori, J. Meinecke, M. C. Levy, M. Koenig, A. Spitkovsky, R. D. Petrasso, C. K. Li, H. Sio, B. Lahmann, A. B. Zylstra, and H.-S. Park, *Phys. Rev. Lett.* **118**, 185003 (2017).
- [23] P. T. Rumsby, J. W. M. Paul, and M. M. Masoud, *Plasma Phys.* **16**, 969 (1974).
- [24] S. M. Pollaine, R. L. Berger, and C. J. Keane, *Phys. Fluids B* **4**, 989 (1992).
- [25] A. S. Wan, T. W. Barbee, R. Cauble, P. Celliers, L. B. DaSilva, J. C. Moreno, P. W. Rambo, G. F. Stone, J. E. Trebes, and F. Weber, *Phys. Rev. E* **55**, 6293 (1997).
- [26] A. J. Harvey-Thompson, S. V. Lebedev, S. Patankar, S. N. Bland, G. Burdiak, J. P. Chittenden, A. Colaitis, P. De Grouchy, H. W. Doyle, G. N. Hall, E. Khoory, M. Hohenberger, L. Pickworth, F. Suzuki-Vidal, R. A. Smith, J. Skidmore, L. Suttle, and G. F. Swadling, *Phys. Rev. Lett.* **108**, 145002 (2012).
- [27] D. D. Ryutov, N. L. Kugland, H.-S. Park, C. Plechaty, B. A. Remington, and J. S. Ross, *Phys. Plasmas* **19**, 074501 (2012).
- [28] M. Casanova, O. Larroche, and J.-P. Matte, *Phys. Rev. Lett.* **67**, 2143 (1991).
- [29] R. L. Berger, J. R. Albritton, C. J. Randall, E. A. Williams, W. L. Kruer, A. B. Langdon, and C. J. Hanna,

- Phys. Fluids B **3**, 3 (1991).
- [30] F. Vidal, J. P. Matte, M. Casanova, and O. Larroche, Phys. Fluids B **5**, 3182 (1993).
 - [31] B. D. Keenan, A. N. Simakov, L. Chacon, and W. T. Taitano, Phys. Rev. E **96**, 053203 (2017).
 - [32] B. D. Keenan, A. N. Simakov, W. T. Taitano, and L. Chacon, Phys. Plasmas **25**, 032103 (2018).
 - [33] S. C. Hsu, T. J. Awe, S. Brockington, A. Case, J. T. Cassibry, G. Kagan, S. J. Messer, M. Stanic, X. Tang, D. R. Welch, and F. D. Witherspoon, IEEE Trans. Plasma Sci. **40**, 1287 (2012).
 - [34] S. C. Hsu, S. J. Langendorf, K. C. Yates, J. P. Dunn, S. Brockington, A. Case, E. Cruz, F. D. Witherspoon, M. A. Gilmore, J. T. Cassibry, R. Samulyak, P. Stoltz, K. Schillo, W. Shih, K. Beckwith, and Y. C. F. Thio, IEEE Trans. Plasma Sci. (2018), DOI: 10.1109/TPS.2017.2774248.
 - [35] S. C. Hsu, A. L. Moser, E. C. Merritt, C. S. Adams, J. P. Dunn, S. Brockington, A. Case, M. Gilmore, A. G. Lynn, S. J. Messer, and F. D. Witherspoon, J. Plasma Phys. **81**, 345810201 (2015).
 - [36] F. D. Witherspoon, S. Brockington, A. Case, E. Cruz, M. Luna, and Y. C. F. Thio, Bull. Amer. Phys. Soc. **62**, 324 (2017).
 - [37] S. C. Hsu, E. C. Merritt, A. L. Moser, T. J. Awe, S. J. E. Brockington, J. S. Davis, C. S. Adams, A. Case, J. T. Cassibry, J. P. Dunn, M. A. Gilmore, A. G. Lynn, S. J. Messer, and F. D. Witherspoon, Phys. Plasmas **19**, 123514 (2012).
 - [38] E. C. Merritt, A. G. Lynn, M. A. Gilmore, and S. C. Hsu, Rev. Sci. Instrum. **83**, 033506 (2012).
 - [39] J. J. MacFarlane, I. E. Golovkin, P. R. Woodruff, D. R. Welch, B. V. Oliver, T. A. Mehlhorn, and R. B. Campbell, in *Inertial Fusion Sciences and Applications 2003*, edited by B. A. Hammel, D. D. Meyerhofer, and J. Meyer-ter-Vehn (American Nuclear Society, 2004) p. 457.
 - [40] J. D. Huba, NRL Plasma Formulary (2016).
 - [41] S. Messer, A. Case, L. Wu, S. Brockington, and F. D. Witherspoon, Phys. Plasmas **20**, 032306 (2013).
 - [42] See supplemental material at [URL will be inserted by publisher] for derivation of Eq. (2).
 - [43] H. W. Liepmann and A. Roshko, *Elements of Gasdynamics* (Wiley, New York, 1957) p. 60.
 - [44] C. Thoma, D. R. Welch, R. E. Clark, N. Bruner, J. J. MacFarlane, and I. E. Golovkin, Phys. Plasmas **18**, 103507 (2011).
 - [45] C. Thoma, D. Welch, R. Clark, D. Rose, and I. Golovkin, Phys. Plasmas **24**, 062707 (2017).